INT. J. NUM. METH. HEAT FLUID FLOW, VOL. 6, 13–20 (1996)

OSCILLATORY FLOW CONVECTION IN A MELTED POOL

D. MORVAN AND PH. BOURNOT

Institut de Recherche sur les Phénomènes Hors Équilibre, Unité mixte CNRS-Universités d'Aix-Marseille 1 et 2 no 138, IMT Technopôle de Château Gombert, 13451 Marseille cedex 20 France

ABSTRACT

A two-dimensional laser surface remelting problem is numerically simulated. The mathematical formulation of this multiphase problem is obtained using a continuum model, constructed from classical mixture theory. This formulation permits the construction of a set of continuum conservation equations for pure or binary, solid-liquid phase change systems. The numerical resolution of this set of coupled partial differential equations is performed using a finite volume method associated with a PISO algorithm. The numerical results show the modifications caused by an increase of the free surface shear stress (represented by the Reynolds number R_e) upon the stability of the thermocapillary flow in the melting pool. The solutions exhibit a symmetry-breaking flow transition, oscillatory behaviour at higher values of R_e. Spectral analysis of temperature and velocity signals for particular points situated in the melted pool, show that these oscillations are at first mono-periodic then new frequencies appear generating a quasi-periodic behaviour. These oscillations of the flow in the melted pool could induce the deformation of the free surface which in turn could explain the formation of surface ripples observed during laser surface treatments (surface remelting, cladding) or laser welding.

KEY WORDS Oscillatory flow Convection Melted pool Multiphase

INTRODUCTION

The engineering applications of high power lasers has appreciably increased during the past decade. The main reason for this development is the potential for this tool to deposit a high energy density with high precision and therefore to perform accurate and very localized operations[1]. The most developed applications of high power lasers involve cutting and drilling where the beam energy is used to vaporize a small piece of material. Another application involves laser welding where both melting and vaporization phenomenon are involved. In this case the advantage of the laser is the possibility to operate in a normal atmosphere which is not the case for other techniques such as electron beam welding. Nevertheless, the development of industrial applications of high power lasers is actually limited when the process induces a melting in a portion of the material. This is caused by the lack of understanding of the physical mechanisms, particularly the hydrodynamic effects which are present in the melted pool. For example, during thermal surface treatments such as surface remelting, cladding and alloying, the convective motions which develop in the melted pool are very important and affect significantly the heat transfer and the phase change. These convective motions result from the surface tension gradient produced by the free surface temperature distribution. For particular conditions the free surface can undergo large deformations which may persist after resolidification creating a surface rippling state[2]. The development of oscillatory flow regimes is also an instability factor for the free surface.

In this paper we present a numerical study of the various flow regimes which could appear in a two-dimensional melted pool model (see *Figure 1*). The free surface shear stress condition

0961–5539/96/010013–08$2.00

Received June 1994
Revised May 1995

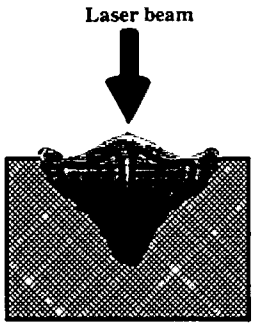

Figure 1 Melted pool geometry model

appears to be the most important factor which controls the development of these hydrodynamical instabilities. This physical parameter is represented by a Reynolds number constructed from a thermocapillary velocity scale and the laser beam diameter

MATHEMATICAL FORMULATION

The mathematical model is constructed from a continuum formulation[3,4], based on the integration of semiempirical laws and microscopic descriptions of transport behaviour with principles of classical mixture theory. This formulation permits the treatment of various solidification problems involving pure and alloy materials, without the need of imposing boundary conditions at the melting front. Therefore, the problem can be solved with a fixed cartesian mesh, reducing the computation time[5,6]. The mathematical model is based on the following assumptions:

- The flow of the molten material is laminar and quasi incompressible (Boussinesq approximation).
- The specific heat is constant inside each phase (these values can be different however in the liquid and in the solid phase).
- The friction forces between the liquid and the solid phase are modelled by a Darcian term which is usually used for incompressible flow in porous media.
- The surface of the target is flat (this is also true for the free surface) and adiabatic outside the interaction zone limited by the laser beam diameter.

Using these assumptions, the present problem can be mathematically defined by the following continuity, momentum and energy equations[7],

$$\frac{\partial}{\partial t}(\rho)+\frac{\partial}{\partial x_j}(\rho v_j)=0 \tag{1}$$

$$\frac{\partial}{\partial t}(\rho v_i)+\frac{\partial}{\partial x_j}(\rho v_j v_i)=-\frac{\partial p}{\partial x_i}+\frac{\partial}{\partial x_i}\left(\mu\frac{\rho}{\rho_l}\frac{\partial v_i}{\partial x_j}\right)+\rho_l g_i\beta(T-T_f)-\frac{\mu}{K}\frac{\rho}{\rho_l}(v_i-v_i^s) \tag{2}$$

$$\frac{\partial}{\partial t}(\rho h)+\frac{\partial}{\partial x_j}(\rho v_j h)=\frac{\partial}{\partial x_j}\left(\frac{k}{c_s}\frac{\partial h_s}{\partial x_j}\right)-\frac{\partial}{\partial h x_j}(\rho(h_l-h)(v_j-v_j^s)) \tag{3}$$

The boundary conditions associated with this problem are,

- West, south and east boundaries:

$$v_j=0 \qquad T=T_0 \tag{4}$$

- North boundary (free surface)

$$\frac{\partial T}{\partial n} = -\frac{q}{k} \tag{5}$$

$$\frac{\partial (v_j \cdot \tau_j)}{\partial n} = \frac{1}{\mu}\frac{\partial \sigma}{\partial \tau} \quad \text{(liquid phase)}$$

$$v_j = 0 \quad \text{(solid phase)} \tag{6}$$

The different variables introduced in the previous equations are,

- ρ_ϕ, c_ϕ, k_ϕ density, specific heat and conductivity in the solid ($\phi = s$) and in the liquid phase ($\phi = l$)
- g_i, β gravitational acceleration and thermal coefficient of expansion
- h_ϕ, v_i^ϕ enthalpy and velocity components in the solid and liquid phases
- p, K, μ pressure, permeability and kinetic viscosity
- g_s, f_s volume and mass fraction of the solid phase
- σ, h_f surface tension and latent heat of fusion,
- T_0 and T_f ambient and melt temperatures
- τ and n tangential and normal directions at the free surface

The mixture density, velocity, enthalpy and thermal conductivity are, respectively,

$$\rho = g_s\rho_s + (1-g_s)\rho_l \tag{7}$$

$$v_j = (1-f_s)v_j^l \tag{8}$$

$$h = f_s h_s + (1-f_s)h_l \tag{9}$$

$$k = g_s k_s + (1-g_s)k_l \tag{10}$$

The enthalpy of the solid and liquid phases are,

$$h_s = c_s T \tag{11}$$

$$h_l = c_l T + [(c_s - c_l)T_f + h_f] \tag{12}$$

The permeability appearing in the momentum equations is assumed to vary with the liquid volume fraction according to the Carman-Kozeny equation,

$$K = K_0\left[\frac{g_l^3}{(1-g_l)^2}\right] \tag{13}$$

where the constant K_0 depends upon the specific structure of the multiphase region.

Numerical solution of the system is performed using a finite volume method, with an implicit Euler scheme for the time discretization and a power law scheme for the evaluation of the interface flux between two neighbouring control volumes[8,9].

The coupling between the pressure and the velocity field is solved with a non-iterative PISO algorithm[10,11]. These different numerical integrations applied for each transport equation which constitutes the physical problem, lead to the final set discretization equations which can be written in a generalized form:

$$a_p\phi_p = \sum_{nb} a_{nb}\phi_{nb} + b \tag{14}$$

where the subscript nb denotes the neighbour grid points of the point P situated at the centre of each computing cell. The linearized equations are then solved using a tridiagonal matrix algorithm (TDMA)[8].

The computational procedure is similar to that described in Reference 9. At the beginning of the problem, the temperature field is evaluated as if it was that of a pure conductive problem

(convective motions are neglected), then the complete problem is solved iteratively for each time step until the following convergence criteria is met,

$$\sqrt{\frac{1}{N}\frac{\sum|\phi^{new}-\phi^{old}|^2}{\max|\phi^{new}|}} \leqslant 10^{-4} \quad \text{for velocities and temperature field} \tag{15}$$

The target dimensions are fixed at $10 \times d$ (d: beam diameter) in the width direction and $5 \times d$ in depth. The aim of the present study is the numerical prediction of unsteady heat and fluid flow in melted pool heated with a steady laser beam. The observation of such hydrodynamical instabilities is necessary associated with asymmetric flow patterns (this phenomena is comparable with the development of a Karman vortex street for a flow around a cylinder). To limit the numerical diffusivity introduced by the power law scheme, a relatively fine grid (126×100) is used with refinement of the mesh near the laser-matter interaction zone where higher temperature gradient and shear stress are observed. This precision is necessary to represent correctly the position of the melt front which is not known at the beginning of the resolution. The calculations are performed with a reduced time step fixed at 0.1. For each solution we have verified that the numerical parameters (grid scales, time step) do not affect the dynamic of the heat and the fluid flow. The governing equations (1–3) are nondimensionalized using the following reference scales,

- length: beam diameter d
- temperature: $\Delta T = T_f - T_0$
- density, specific heat and conductivity: ρ_l, c_s and k_l
- velocity:

$$U = \sqrt{\frac{\gamma \Delta T}{\rho d}} \quad \text{with } \gamma = |\mathrm{d}\sigma/\mathrm{d}T|$$

- enthalpy: $c_s(T_f - T_0)$

The dimensionless variables are,

$$x_j^* = \frac{x_j}{d}, \qquad t^* = \frac{tU}{d}, \qquad v_j^* = \frac{v_j}{U}, \qquad T^* \frac{T}{\Delta T} \tag{16}$$

$$h^* = c_l^* T^* + (1 - c_l^*) T_f^* + \frac{1}{S_{te}} \tag{17}$$

$$\rho^* = \frac{\rho}{\rho_l}, \qquad k^* = \frac{k}{k_l}, \qquad c_\phi^* = \frac{c_\phi}{c_s} \tag{18}$$

Introducing these dimensionless variables, the governing equations and side conditions of the problem is as follows,

$$\frac{\partial}{\partial t^*}(\rho^*) + \frac{\partial}{\partial x_j^*}(\rho^* v_j^*) = 0 \tag{19}$$

$$\frac{\partial}{\partial t^*}(\rho^* v_i^*) + \frac{\partial}{\partial x_j^*}(\rho^* v_j^* v_i^*) = -\frac{\partial p^*}{\partial x_i^*} + \frac{\partial}{\partial x_j^*}\left(\frac{\rho^*}{R_e}\frac{\partial v_j^*}{\partial x_j^*}\right) - \frac{G_r}{R_e^2}(T^* - T_f^*)\delta_{i2} - \frac{1}{R_e D_a}\frac{\rho^*}{K^*}(v_i^* - v_i^{*s}) \tag{20}$$

$$\frac{\partial}{\partial t^*}(\rho^* h^*) + \frac{\partial}{\partial x_j^*}(\rho^* v_j^* h^*) = \frac{\partial}{\partial x_j^*}\left(\frac{k^*}{R_e P_r}\frac{\partial h_s^*}{\partial x_j^*}\right) - \frac{\partial}{\partial x_j^*}(\rho^*(h_l^* - h^*)(v_j^* - v_j^{*s})) \tag{21}$$

The corresponding boundary conditions are,

- West, south and east boundary:

$$T^* = T_0^* \quad \text{and} \quad v_j^* = 0 \tag{22}$$

- North boundary:

$$\frac{\partial T^*}{\partial n^*} = -\frac{q^*}{k^*} \tag{23}$$

$$\frac{\partial v_j^* \cdot \tau^*}{\partial n^*} = \text{sign}(\gamma)\, Re \frac{\partial T^*}{\partial \tau^*} \quad \text{for the liquid phase}$$

$$v_j^* = 0 \quad \text{for the solid phase} \tag{24}$$

The physical system is therefore completely defined with five non-dimensional parameters,

- the Reynolds, Prandtl and Grashof numbers:

$$R_e = \frac{\rho_l U d}{\mu} \qquad G_r = \frac{g\beta \Delta T d^3 \rho_l^2}{\mu^2} \tag{25}$$

$$P_r = \frac{\mu c_s}{k_l} \tag{26}$$

- the Darcy and Stefan numbers

$$D_a = \frac{K}{d^2} \qquad S_{te} = \frac{c_s \Delta T}{h_f} \tag{27}$$

NUMERICAL RESULTS AND DISCUSSION

In this study we analyze the effects of an increase of the free surface shear stress upon the stability of the flow inside the melted pool. For this thermal configuration (the heat source is located at the top of the melted pool), the thermocapillary convection is much more important than the natural convection. Therefore we have assumed that the effects of the Grashof number could be neglected. The results presented in *Figures 2, 3, 4, 5* show the various flow patterns obtained for different free surface shear stress conditions (the values for the physical parameters are listed on *Table 1*, they represent the conditions for the surface remelting of an aluminium target). For an unsteady solution, the streamlines are represented for only one time (at the beginning of a

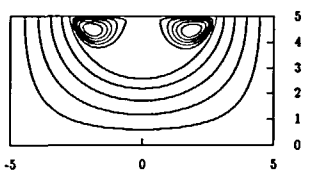

Figure 2 Flow pattern for $R_e = 100$

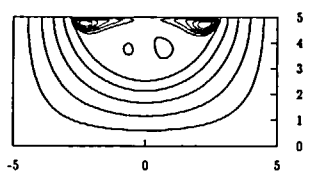

Figure 3 Flow pattern for $R_e = 350$

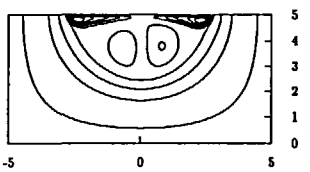

Figure 4 Flow pattern for $R_e = 550$

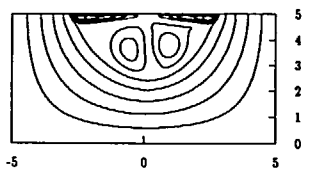

Figure 5 Flow pattern for $R_e = 800$

Table 1 Physical parameters: typical values (Aluminium target)

Physical parameters	Typical values
Reynolds number R_e	10–800
Prandtl number P_r	0.01
Grashof number G_r	0
Stefan number S_{te}	∞
Liquid-solid specific heat ratio c_l/c_s	1.0
Solid-liquid conductivity ratio k_s/k_l	2.4
Solid-liquid density ratio ρ_s/ρ_l	1.0
Dimensionless heat flux $qd/k_l\Delta t$	5.0

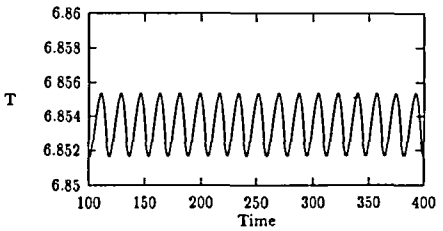

Figure 6 Temperature signal for $R_e = 100$

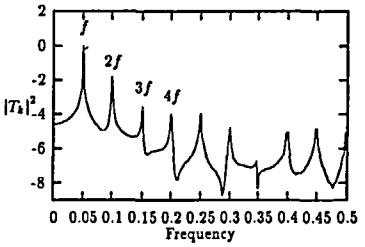

Figure 7 Power spectrum of temperature signal for $R_e = 100$ (logarithmic scale)

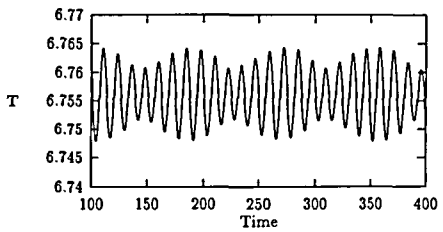

Figure 8 Temperature signal for $R_e = 350$

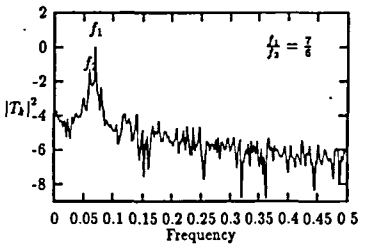

Figure 9 Power spectrum of temperature signal for $R_e = 350$ (logarithmic scale)

cycle for example if the solution is periodic). The streamlines show that an increase of the thermocapillary Reynolds number induces the development of two then four convective cells in the melted pool. From a qualitative point of view, the general structure of the flow is comparable with the results obtained for other neighbouring conditions[12,13]. The convective motions could be separated in two zones. The cells situated near the free surface are symmetric, the distance which separate each streamline indicate that the intensity of the velocity is higher near the free surface than at the bottom of the melted pool. This flow represents the direct contribution of the shear stress generated by the surface tension gradient at the free surface (thermocapillary convection). The cells situated at the bottom of the melted pool are generally asymmetric, for a periodic flow we have observed a periodic growth and decrease of these two cells. The intensity of this secondary flow increases with the Reynolds number. It results from the shear stress induced at the bottom of the melted pool by the thermocapillary convection cells. The symmetrical breaking can be observed for a Reynolds number greater than 100 (*Figures 3, 4, 5*), this flow

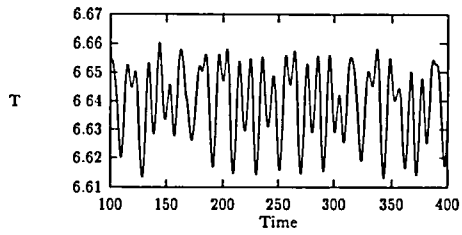

Figure 10 Temperature signal for $R_e = 550$

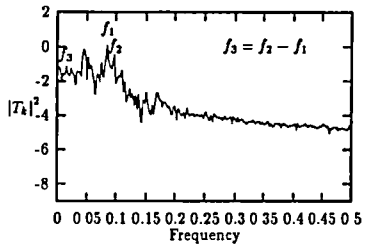

Figure 11 Power spectrum of temperature signal for $R_e = 550$ (logarithmic scale)

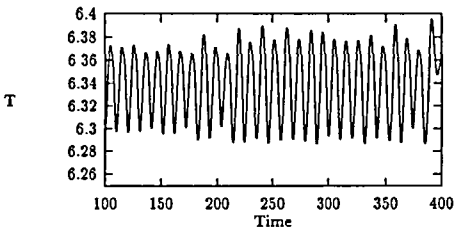

Figure 12 Temperature signal for $R_e = 800$

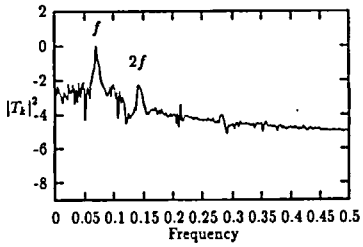

Figure 13 Power spectrum of temperature signal for $R_e = 800$ (logarithmic scale)

pattern is coupled with an oscillatory behaviour as can be seen in the temperature signals (*Figures 6, 8, 10, 12*) and the corresponding power spectrum analysis (*Figures 7, 9, 11, 13*).

For $Re = 100$, the flow in the melted pool has a mono-periodic behaviour (*Figure 6*), characterized by a fundamental frequency $f = 0.05$ followed by its different harmonics (*Figure 7*). For a $Re = 350$, the flow dynamic exhibits a bi-periodic behaviour (*Figures 8, 9*) with two nearly equal frequencies $f_1 = 0.07$ and $f_2 = 0.06$ ($f_1/f_2 = 7/6$) which induce a modulation of the amplitude of the periodic signal.

For higher values of Re, the temperature signal is also bi-periodic ($Re = 550$) with two different frequencies $f_1 = 0.085$ and $f_2 = 0.0975$ associated with the difference $f = f_2 - f_1$ and its harmonics (*Figures 10, 11*). For $Re = 800$ the flow becomes again quasi-monoperiodic with a fundamental frequency $f = 0.07$ (*Figures 12, 13*).

CONCLUSION

As it has been shown by the previous results, the thermocapillary flow in a melted pool exhibits an unsteady behaviour characterized by periodic and quasi-periodic temperature signals. If we compare the average frequency f with the frequency f_s constructed from the interaction time for a laser processing, it is clear that for a moving heat source, these oscillations could exist only for small values of scanning velocity. For an aluminium or a steel target the oscillation frequency in the melted pool f could vary from 10 to 20 Hz. This should be compared with the values of $f_s = V_s/d = 1$ Hz $-$ 1 kHz (for a scanning velocity 1 mm/s $< V_s <$ 1 m/s and a beam diameter $d = 1$ mm). The formation of surface ripples observed during real laser applications (surface remelting, cladding, welding) could also be produced by other source of melted pool oscillations, induced by unsteady thermal coupling between the laser beam and the target (plasma formation, variation of the absorption coefficient). Nevertheless these results must be confirmed by experimental investigations, it is quite possible that in the real cases where the free surface can be deformed, the oscillations in the melted pool will be suppressed.

ACKNOWLEDGEMENTS

The computation were carried out on a Cray Y-MP computer with support from Centre Régional de Calcul et de Télécommunications Scientifiques. Research support from MICE (Eurêka EU-194), CNRS and région PACA in France is gratefully acknowledged.

REFERENCES

1 Tanasawa, I. and Lior, N. (eds.) *Heat and Mass Transfer in Material Processing*, 81–106, Springer-Verlag, Berlin Heidelberg (1987)
2 Anthony, T. R. and Cline, H. E. Surface rippling induced by surface-tension gradients during laser surface melting and alloying, *J. Appl. Phys.*, **48** (9), 3888–3894 (1977)
3 Bennon, W. D. and Incropera, F. P. A continuum model for momentum, heat and species transport in binary solid-liquid phase change systems: 1, Model formulation, *Int. J. Heat Mass Transfer*, **30** (10), 2161–2170 (1987)
4 Bennon, W. D. and Incropera, F. P. A continuum model for momentum, heat and species transport in binary solid-liquid phase change systems: 2 Application to solidification in a rectangular cavity, *Int. J. Heat Mass Transfer*, **30** (10), 2171–2187 (1987)
5 Bennon, W. D. and Incropera, F. P. Numerical analysis of binary solid-liquid phase change using a continuum model, *Num. Heat Transfer*, **13**, 277–296 (1988)
6 Voller, V. R. and Prakash, C. A fixed grid numerical modelling methodology for convection-diffusion mushy region phase change problems, *Int. J. Heat Mass Transfer*, **30** (8), 1709–1719 (1987)
7 Morvan, D. and Bournot, Ph. Simulation numérique de la convection thermocapillaire dans un bain de fusion, In *Actes du 11 eme Congrès Français de Mécanique*, **2**, 21–24, Villeneuve d'Ascq, 6–10 Septembre 1993. Presses de l'Université de Lille III
8 Patankar, S. V. A calculation procedure for two-dimensional elliptic situations, *Num. Heat Transfer*, **4**, 409–425 (1981)
9 Van Doormaal, J. P. and Raithby, G. D. Enhancements of the SIMPLE method for predicting incompressible fluid flow. *Num. Heat Transfer*, **7**, 147–163 (1984)
10 Issa, R. I., Gosman, A. D. and Watkins, A. P. The computation of compressible and incompressible recirculating flows by a non-iterative implicit scheme, *J. Comput. Physics*, **62**, 66–82 (1986)
11 Jang, D. S., Jetli, R. and Acharya, S. Comparison of the PISO, SIMPLER and SIMPLEC algorithms for the treatment of the pressure-velocity coupling in steady flow problems, *Num. Heat Transfer*, **10**, 209–228 (1986)
12 Basu, B. and Srinivasan, J. Numerical study of steady state laser melting problem, *Int. J. Heat Mass Transfer*, **31** (11), 2331–2338 (1988)
13 Kanouff, M. and Grief, R. The unsteady development of a GTA weld pool, *Int. J. Heat Mass Transfer*, **35** (1), 967–979 (1992)